International Journal of Mechanical Sciences 285 (2025) 109790

Contents lists available at ScienceDirect

International Journal of Mechanical Sciences

journal homepage: www.elsevier.com/locate/ijmecsci

Attenuation of Lamb waves in coupled-resonator viscoelastic waveguide

Yu-Ke Ma [a,1], Wei Guo [a,b,1], Yi-Ming Cui [a], Yan-Feng Wang [a,c,*], Vincent Laude [d], Yue-Sheng Wang [a,e]

[a] School of Mechanical Engineering, Tianjin University, 300350 Tianjin, China
[b] China United Engineering Corporation Limited, Hangzhou 310000, China
[c] National Key Laboratory of Vehicle Power System, Tianjin 300350, China
[d] Institut FEMTO-ST, CNRS, Université Bourgogne Franche-Comté, Besançon 25030, France
[e] Institute of Engineering Mechanics, Beijing Jiaotong University, Beijing 100044, China

ARTICLE INFO

Keywords:
Lamb wave
Coupled resonator viscoelastic waveguide
Kelvin–Voigt model
Complex band structure
Theoretical prediction

ABSTRACT

Guidance of elastic waves is one of the main applications of artificial crystal structures. The attenuation of the guided waves is, however, often overlooked, as most of the proposed waveguides only comprise ideal elastic materials. In this work, we study the propagation of evanescent Lamb waves guided in coupled-resonator viscoelastic waveguide (CRVW), with special attention to attenuation. CRVW is defined by considering a linear chain of coupled defect cavities in a phononic plate made of epoxy. The viscoelastic behavior of epoxy is characterized numerically by the Kelvin–Voigt (K–V) model. Based on finite element analysis, the complex band structure and the spectrum of frequency response function (FRF) are obtained. Due to viscosity, guided Lamb waves are spatially damped. Two theoretical models are devised to predict the displacement distributions inside and outside a bandgap for guided waves, respectively, considering either the first or the first two least evanescent Bloch waves identified in the complex band structure. A CRVW sample is fabricated and characterized experimentally by laser vibrometry. Evanescent Lamb waves are observed to be strongly confined along the waveguide and at the same time to decay rapidly along the waveguide axis. Experiments and numerical simulations are found to be in fair agreement. The present work is expected to inspire practical applications of highly confined viscoelastic phononic waveguides.

1. Introduction

Along the last decades, the study of elastic wave propagation in structured materials has attracted a great deal of attention [1–4]. As a functional composite material with spatial periodicity, phononic crystal (PC) relies on highly contrasting elastic moduli and mass densities. Spatial modulation on a scale comparable to the wavelength leads to many salient properties, such as bandgaps [5–8] and band-edge states [9]. The main mechanisms for bandgap generation are Bragg scattering and local resonance [10,11]. In the frequency range of a bandgap, propagation of elastic/sound waves is prohibited, and only evanescent waves are allowed [12,13]. This property allows PCs to be used for sound absorption [14,15], vibration damping [16,17], or filtering [18,19].

The modification of an individual or of a series of unit cells in the periodic structure of a PC disrupts the original periodicity and results in the formation of point, line or surface defects [20–22]. Defective bands can in turn appear in the frequency range of the original bandgap. The waves forming the defective dispersion bands are confined to the defects and propagate along the designed structural defects. Hence, wave propagation can be controlled or manipulated by designing defects [23–25]. When defects are close enough, coupling effects occur between them, leading to the formation of coupled resonator waveguides [26–28]. Unlike linear waveguides, coupled-resonator waveguides are based on the evanescent wave coupling mechanism [29,30] between defective cavities or resonators, which theoretically allows for the design of arbitrary acoustic lines [31]. Coupled-resonator waveguides are extremely sensitive to local variations in the defective cavities or resonators, such as their separation or the amount of prestress at the defect [32,33]. The dispersion relation is ultimately determined by the coupling strength between the defective cavities or resonators [34].

Attention to linear/coupled-resonator waveguides for manipulation of elastic or sound waves has increased considerably in recent years [26,35–39]. Shi et al. [35] designed a compact and frequency-robust waveguide squeezed by two layers of metagratings with only

* Corresponding author at: School of Mechanical Engineering, Tianjin University, 300350 Tianjin, China.
E-mail address: wangyanfeng@tju.edu.cn (Y.-F. Wang).
[1] Yu-Ke Ma and Wei Guo contributed equally to this work.

https://doi.org/10.1016/j.ijmecsci.2024.109790
Received 31 May 2024; Received in revised form 29 September 2024; Accepted 13 October 2024
Available online 19 October 2024

one identical unit cell. They found that flexural waves can be efficiently guided by the waveguide. Jiang et al. [40] realized interface transport by replacing defects in acoustic valley insulators to form an acoustic waveguide. Hatanaka et al. [41] designed a phononic waveguide by using a one-dimensional array of suspended membranes that integrates isolated nanoelectromechanical systems. Wang et al. [42] created reconfigurable coupled-resonator acoustoelastic waveguides consisting of a periodic array of cups selectively filled with water. They showed that acoustoelastic waves can be controlled by locally removing water from certain cups. Most of the existing studies, however, only consider an elastic model and do not involve viscoelastic materials.

In viscoelastic media, the dissipation of waves cannot be ignored. The presence of viscosity can have an effect on the dispersion of waves in PCs [43–48]. For example, for PCs made of rubber and epoxy resin, frequency dispersion and energy dissipation occur when waves propagate in the viscoelastic medium [13,49,50]. Recently, some studies have been conducted on the effects of viscoelasticity on wave dispersion. Laude et al. [51] theoretically analyzed the effect of loss on the dispersion relation of waves in viscoelastic phononic and photonic crystals. Moiseyenko et al. [44] investigated the effect of a linear increase in material viscosity with frequency on the complex energy band structure of two-dimensional viscoelastic PCs. Zhang et al. [46] discussed wave attenuation in locally resonant viscoelastic PCs. Viscoelastic damping reduces the attenuation in the bandgap and increases the attenuation bandwidth. By optimizing the design structure, it is possible to change the bandwidth and reduce the attenuation of the locally resonator bandgap (LRBG) [52], but there is no effect on the position of the bandgap [53]. Oh et al. [54] investigated wave attenuation and dissipation mechanisms in viscoelastic PCs with different inclusions for the long-wavelength regime. Yip and John [55] described the trapping and absorption of audible sound in centimeter-scale claddings of two-dimensional, locally resonant viscoelastic phononic crystals. Viscoelasticity is usually analyzed using linear viscoelastic models, including the generalized Maxwell model [52] and the Kelvin–Voigt (K–V) model [56–60]. The K–V model, that is adopted in this paper, is conveniently represented in the frequency domain using complex stiffness with a fixed real part and an imaginary part varying linearly with frequency. The K–V model can correctly characterize the properties of viscoelastic materials [61–64]. Although the papers mentioned above investigated wave attenuation in viscoelastic PCs, evanescent guided Lamb waves in waveguides consisting of defects in a PC plate have seldom been studied. Furthermore, few experiment has been conducted to observe the decay of evanescent waves and to compare it with numerical results. It is thus difficult to characterize thoroughly the propagation and attenuation characteristics of evanescent waves. Based on this, using numerical simulation to accurately predict the behavior of evanescent guided waves in viscoelastic waveguides remains a challenge in practice. This task is essential to modern applications of waveguides that often comprise viscoelastic materials.

In this paper, we design and fabricate a coupled-resonator viscoelastic waveguide (CRVW) using epoxy as the base material. The CRVW is formed by filling certain of the cross holes in the crystal to form a sequence of defect cavities. We focus on the propagation and the attenuation of guided waves. The viscoelastic behavior is accounted for numerically by considering the K–V model. The complex band structure and FRF are first calculated and discussed. Experimental measurements are carried out by using a scanning vibrometer. The displacement distribution of evanescent Bloch waves inside and outside the bandgap is modeled based theoretical models inspired by diffraction theory and the model of the channeled spectrum from optics. It is observed that guided Lamb waves propagating along defects are strongly confined in the lateral direction. Guided Lamb waves are spatially evanescent and show a strong attenuation along the CRVW. Both numerical and experimental results agree fairly well with the two models. Waveguides made of epoxy are expected to provide non-destructive testing for viscoelastic materials and mitigation of unwanted elastic waves emitted by sources of elastic waves. This paper provides a basis for the design and practical application of highly confined viscoelastic phononic devices.

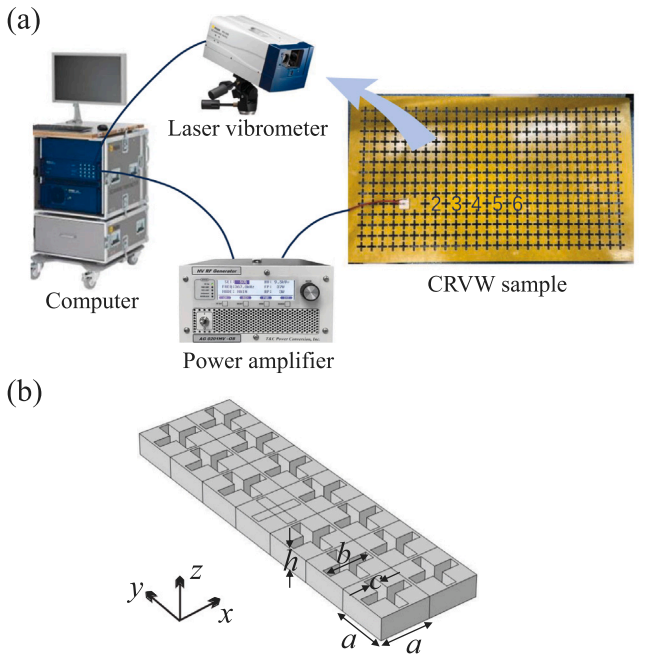

Fig. 1. Coupled-resonator viscoelastic waveguide using epoxy as the base material. (a) Lamb wave propagation is imaged at the source frequency using a laser vibrometer sensitive to vertical displacements. Defects forming the waveguide are numbered sequentially from 2 to 6. (b) The supercell of the CRVW includes one defect every two periods of the crystal of cross holes. Geometric parameters for the sample are $a = 20$ mm, $b/a = 0.9$, $c/a = 0.2$, and $h/a = 0.4$.

2. Methods

The experimental setup for measuring the out-of-plane vibrations of the surface of the CRVW sample is shown in Fig. 1(a). The sample is manufactured by mechanical machining of an epoxy plate with a thickness of 8 mm. The crystal is composed of a square-lattice arrangement of cross holes, which is known to induce a wide complete band gap. The CRVW design is a straight chain of defect cavities separated by 2 lattice constants, as Fig. 1(b) shows. Defects are simply introduced by omitting the machining of cross holes inside the considered unit-cells. An asymmetric wave source is formed by a vertically-polarized piezoelectric patch glued on one side of the plate, in view of favoring the excitation of out-of-plane vibrations. The electrical driving signal is first amplified before being applied to the piezoelectric patch. Note that the excitation is applied on an homogeneous part of the plate and is positioned away from the external boundaries, in order to prevent elastic waves from reverberating on them. This arrangement favors the excitation of the chain of defect cavities. A Polytec PSV-500 scanning laser vibrometer is used to measure the out-of-plane displacement distribution along and around the waveguide. In the experiments, the laser is first moved to approximately the middle of the sample under test and is focused on the surface. Then two-dimensional alignment is performed to establish the relationship between the pixel position in the image and the laser swing angle. After the laser is calibrated, the laser vibrometer is used to measure the bandgap of a perfect PC plate to ensure experimental consistency and to calibrate the measurements. The frequency response is detected by applying a periodic chirp signal and by measuring the displacement at the central parts over the same area for the defects designated in Fig. 1(a). The signal sweeps from 45 kHz to 70 kHz, with 3200 sample points. The displacement field over the surface of the plate is measured by using a harmonic signal with a selected frequency.

Numerical simulations are conducted using finite element analysis, with software COMSOL Multiphysics. The supercell in Fig. 1(b) is

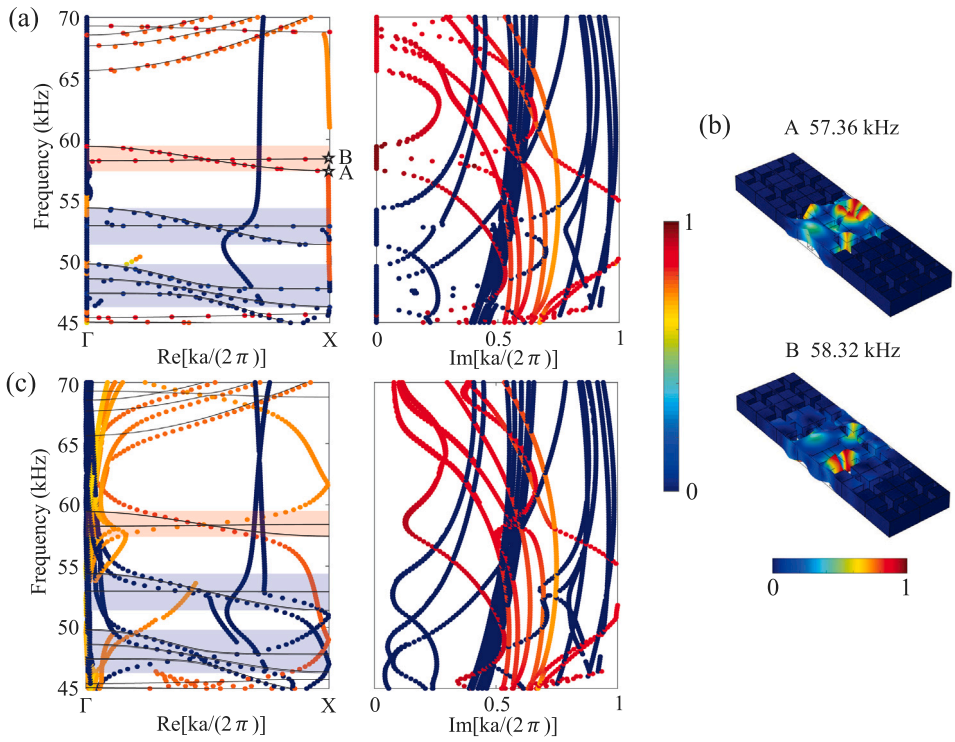

Fig. 2. Finite element analysis of dispersion and attenuation in CRVW. Panel (a) presents the complex band structure computed using the elastic model. The left and right panels show the variation of frequency with real and imaginary parts of the wavenumber, respectively. The color scale measures the polarization of waves from in-plane (blue) to out-of-plane (red). The black solid line is the real band structure. The light red and blue areas highlight the frequency ranges for out-of-plane and in-plane polarized guided waves, respectively. Panel (b) shows the out-of-plane displacement for eigenmodes A and B. The color scale indicates the normalized amplitude of out-of-plane displacements from 0 (blue) to 1 (red). Panel (c) presents the complex band structures obtained by considering the viscoelastic model.

used to obtain the dispersion relation of guided Bloch waves. Epoxy is considered isotropic, with mass density $\rho = 2038$ kg/m^3, Poisson's ratio $\nu = 0.41$, and Young's modulus $E = 24$ GPa. The complex band structure in particular is of great significance to understand in depth wave propagation. Viscoelasticity is represented with the K–V model. The frequency-dependent loss is thus added to the imaginary part of the modulus. The complex-valued stiffness tensor is

$$\mathbf{C}^{v} = \mathbf{C} + \iota\omega\boldsymbol{\eta} \tag{1}$$

where $\mathbf{C}$ is the usual real-valued elastic tensor and $\boldsymbol{\eta}$ is the viscosity tensor with the same symmetry as the $\mathbf{C}$ [13]. Details of the finite element analysis can be found in Ref. [65]. Since propagation of Lamb waves in a two-dimensional phononic periodic plate is studied in this paper, periodic boundary conditions are applied along the x and y directions, whereas they were only applied along the x direction in Ref. [65], in which a phononic crystal strip was modeled. The remaining surfaces are left free. Complex band structures are obtained by sweeping the angular frequency ω in the range of interest while choosing wavenumber k as the eigenvalue. Alternatively, the real band structure is obtained by sweeping k along the boundary of the irreducible Brillouin zone, considering ω as the eigenvalue. The distribution of displacement for a specific eigenmode is obtained from the eigenvector.

For comparison with experiment, we further calculate the frequency response function (FRF) by building a time-harmonic model of the finite plate. A z-polarization displacement wave source with unit amplitude is applied to the left homogeneous part of the waveguide. The frequency response function (FRF) is estimated by computing the vertical displacement at a selected region in the computation domain. Integrating over the excitation (S_0) and the receiving regions (S_1), the FRF is

$$\mathrm{FRF}(\omega) = \frac{\int_{S_1} |U| dS}{\int_{S_0} |U| dS} \tag{2}$$

where U is the vertical displacement.

3. Dispersion and attenuation relations of coupled resonator viscoelastic waveguide

In practice, no solid material is ideally elastic or lossless. The presence of viscosity affects the propagation of waves. In this section, the dispersion and the attenuation in coupled-resonator viscoelastic waveguides is analyzed with the finite element method. More precisely, the complex band structure of CRVWs is calculated considering the K–V model of viscoelasticity.

A CRVW is formed by filling certain of the cross holes of the square-lattice crystal to form defect cavities separated by 2 lattice constants, as shown in Fig. 1(b). The complex band structure obtained considering the purely elastic model, i.e. without viscoelasticity, is shown in Fig. 2(b). The complex band structure is presented in two panels: the left (real) panel shows frequency versus the right (imaginary) part of the wavevector. The polarization amount is measured as the ratio of the out-of-plane displacement to the total displacement. It is displayed as a colorscale to distinguish between different modes. For reference, the real band structure is also plotted with black solid lines. The real part of the complex band structure coincides exactly with the real band structure, an indication of the correctness of the calculation of complex band structure. The wide complete bandgap of the perfect crystal extends from 45.27 kHz to 65.14 kHz. Within it, three separated guiding ranges appear in Fig. 2(b). Only the guided waves in the range 57.43 kHz $< f <$ 59.43 kHz are polarized mostly out-of-plane. They are mainly considered in the following analysis, because they are available experimentally. This guiding range is isolated from the two other in-plane guiding ranges. The minimum imaginary parts of the wavevector for guiding bands are uniformly zero, signaling propagation of guided waves without attenuation. Eigenmodes for out-of-plane guided waves at the X point of the first Brillouin zone are shown in Fig. 2(c). The out-of-plane displacement for eigenmode A is symmetrical with respect to the xz plane, i.e. the wave propagation direction. This mode can be

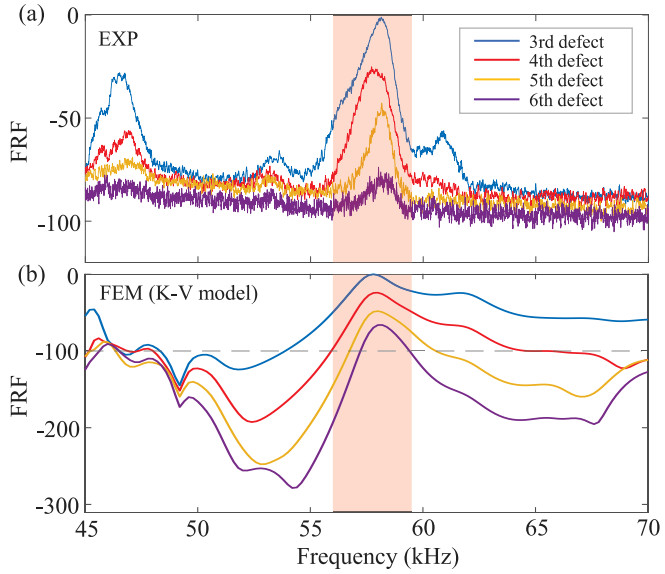

Fig. 3. FRFs obtained from different receiving regions. Panel (a) presents the experimental results measured at the third to the sixth defects (see labels in Fig. 1(a)) with blue, red, yellow and purple lines, respectively. Panel (b) presents the numerical FRFs at the same defects computed using the K–V model. The light red area indicates the frequency range of out-of-plane polarized guided waves. FRFs are normalized to the maximum obtained for the third defect. The black dot line at −100 dB in panel (b) virtually marks the numerical baseline.

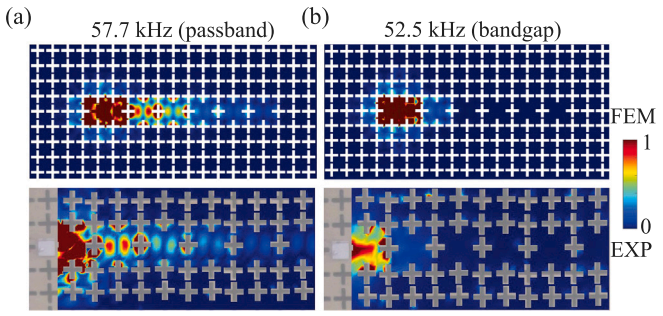

Fig. 4. Displacement field of Lamb waves in the coupled-resonator viscoelastic waveguide. Panels (a) and (b) present the numerical and experimental results for the finite epoxy phononic crystal slab at 57.7 kHz and 52.5 kHz. These frequencies lie inside the guidance frequency range and the complete band gap for out-of-plane waves, respectively. The color scale represents the amplitude of the normalized out-of-plane displacement from 0 (blue) to 1 (red).

excited by an incident symmetric plane wave and is expected to appear in the frequency response. In contrast, the out-of-plane displacement for eigenmode B is asymmetric with respect to the same plane and thus the corresponding band is deaf. Such a mode can hardly be excited by an incident symmetric plane wave.

We then compute the complex band structure by including the K–V model to investigate the effect of viscoelasticity, as Fig. 2(d) presents. The viscosity parameter used for epoxy is $\eta_{44} = 2\times10^3$ Pa s, corresponding to rather large material loss in the considered frequency range. The sharp corners of the complex band structure at the high symmetry points are smoothed and rounded after viscosity is added, resulting in the blurring of the bandgap boundaries. The minimum imaginary parts of wavevector of guided out-of-plane waves are non-zero. As a result, the guided Lamb waves become evanescent. Comparing the imaginary parts in Fig. 2(b) and Fig. 2(d), the effect of viscosity on the lower order evanescent Bloch waves is particularly obvious. They are suitable for studying the attenuation of highly confined Lamb waves, as discussed next.

4. Evanescent waves in coupled-resonator viscoelastic waveguide

In this section, we examine the attenuation of evanescent Lamb waves guided along a CRVW. We measure the FRF at four distinct receiving regions, i.e. the third to sixth defects labeled in Fig. 1(a). Fig. 3(a) show the experimental FRFs. They are consistently normalized by the maximum of the response on the third defect. A guidance frequency range 57.4 kHz $< f <$ 59.3 kHz is apparent in the complete bandgap. With increasing distance from the excitation, the magnitude of the FRF gradually decreases in the guidance frequency range. The marked attenuation confirms the relatively large minimum imaginary part of the wavenumber. Fig. 3(b) shows the numerical FRFs computed considering the K–V model on the same receiving regions as in the experiment. The larger the distance from the excitation, the smaller the FRF obtained with the K–V model. The observed guidance frequency range is consistent with experiment. The numerical and experimental FRFs do not have the same dynamical range, due to the experimental noise floor. Hence, we figure a virtual baseline at −100 dB in the numerical FRF plot of panel (b), to ease the visual comparison. It is consistent with the minimum value of the experimental frequency response. It is observed that the FRFs above the black dot line are in fair agreement with experiment. Besides, a small FRF peak is found experimentally around 53.6 kHz. It might result from the piezoelectric patch being only attached on one side of the plate, causing spurious in-plane waves to be excited and collected [33]. We also computed the FRFs considering the elastic model, i.e. no viscosity. The result, shown in Appendix, deviates markedly from experiment.

In addition to the FRF, it is interesting to image the displacement fields of evanescent waves at chosen frequencies. Fig. 4(a) shows the numerical and experimental displacement distributions at 57.7 kHz that lies inside the guidance frequency range. The guided Lamb wave propagates along the waveguide with a relatively strong attenuation but remains strongly confined in the lateral direction. This wave presents the characteristics of guided evanescent Bloch waves. The displacement field at 52.5 kHz, that lies inside the complete band gap for out-of-plane Lamb waves, is presented in Fig. 4(b). Both simulated and experimental results show that the evanescent Lamb wave concentrates at the defect closest to the excitation. A rapid attenuation of the evanescent waves away from the excitation is observed. As a whole, simulation results based on the K–V model are consistent with experimental measurements. We can thus reasonably characterize the propagation and attenuation of evanescent waves along the viscoelastic waveguide by selecting the K–V model.

To quantitatively assess the spatial decay of evanescent Lamb waves, we extract the displacement distributions along the centerline of the upper surface at the defects, as plotted in Fig. 5 and Fig. 6. The simulated and experimental results can be compared directly within the sequence of coupled defects. As Fig. 5 shows, the agreement at 52.5 kHz, inside the complete band gap, is very good. It is visually observed that the evanescent wave decays rapidly and exponentially. In Fig. 6, at 57.7 kHz, inside the guidance frequency range, the agreement is still excellent for the second defect. For the subsequent defects, the agreement remains fair, especially regarding the amplitudes of the out-of-plane displacement. The slight discrepancies might be attributed to fabrication uncertainties and to the quite crude knowledge of the viscosity of epoxy. The viscosity coefficient considered in the FEM numerical simulation is further homogeneous, which may not be not exactly the case of the actual CRVW sample.

5. Models of the displacement distribution in coupled-resonator viscoelastic waveguide

In this section, we apply two theoretical models inspired by optical diffraction grating theory and the channeled spectrum; they respectively predict the displacement distributions of evanescent Lamb waves inside the band gap and inside the guidance frequency range.

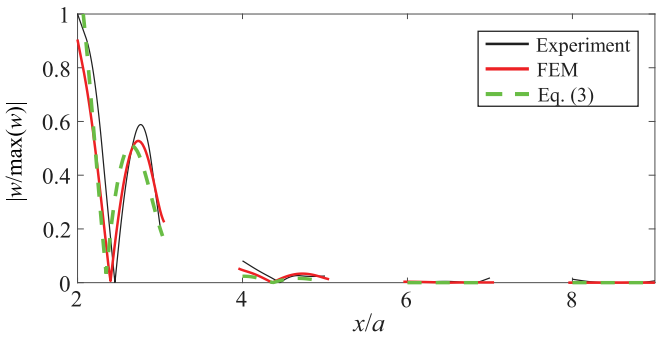

Fig. 5. Attenuation of evanescent waves in CRVW at 52.5 kHz. Displacement distribution of simulation and experiment along the centerline of upper surface at the defects are presented by the red and black solid lines, respectively. The green dashed line represents the displacement distributions predicted with $\phi_1 = 0.1$, $k_1 a/2\pi = 0.52 - 0.45\imath$, $\phi_2 = 0.9$, $k_2 a/2\pi = 0.47 - 0.46\imath$. The blue dashed line represents the displacement decay curve fitted using the minimum imaginary part in the complex band structure.

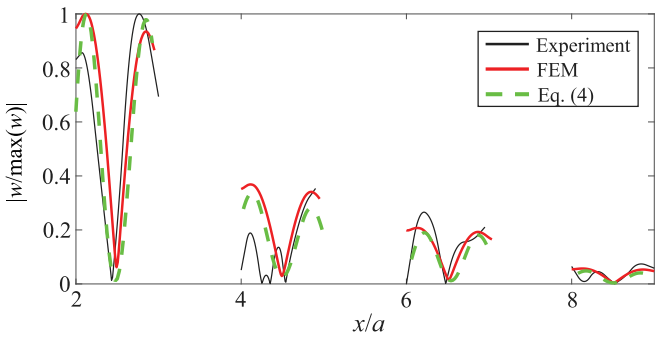

Fig. 6. Attenuation of evanescent waves in CRVW at 57.7 kHz. Displacement distribution of simulation and experiment along the centerline of upper surface at the defects are presented by the red and black solid lines, respectively. The green dashed lines represent the displacement distributions predicted with $ka/2\pi = 0.68 - 0.14\imath$, $\alpha = 1.60 + 0.91\imath$, $\beta = 0.05 - 0.02\imath$.

First, according to diffraction grating theory [12], the diffracted field is composed of a superposition of harmonic waves. From this description, the evanescent field can be represented as a superposition of evanescent waves with different orders of diffraction. Since evanescent waves decay rapidly, it is sufficient in a first approximation to consider only the first two least evanescent orders of diffraction. The evanescent field is hence written described [65]

$$w(x,y) = \phi_1 w_1(x,y)e^{-\imath k_1 x} + \phi_2 w_2(x,y)e^{-\imath k_2 x} \tag{3}$$

where ϕ_i represents the weighting coefficient for each evanescent wave, k_i is the wavenumber and w_i refer to the displacement field extracted from the first and second least evanescent eigenmodes in the complex band structure ($i = 1, 2$). Using this formula, we plot the modeled displacement distribution at 52.5 kHz in Fig. 5. It is found that the model correctly captures the main trends.

Second, the channeled spectrum, that has long been known for optical waveguides, is formed by the interference of forward propagating guided waves and the backward propagating waves generated by internal reflections. The description is here extended to the PC waveguide. The channeled spectrum in CRVW is considered to be generated by the interference of the same guided Bloch wave propagating forward and backward. In the inner part of the waveguide, the right-traveling wave L_r and the left-traveling wave L_l are superimposed to form the displacement field [66]:

$$L(x,y) = \alpha L_r(x,y)e^{-\imath kx} + \beta L_l(x,y)e^{\imath kx} \tag{4}$$

where α and β are complex coefficients to be determined and k is the complex Bloch wavenumber of the waveguide. The left and right traveling waves have periods Λ and satisfy $\overline{L}_r(x,y) = L_l(\Lambda - x, y)$, where $\overline{L}_l(x,y)$ is the conjugate complex number of $L_l(x,y)$. It is noted that the left and right traveling waves transform into each other by reflection at both ends of the PCs structure. We fit the displacement distribution obtained with FEM using Eq. (4). Using this formula, we plot the modeled displacement distribution at 57.7 kHz in Fig. 6. It is observed that the channeled spectrum model correctly captures the main trends. This result will be of great help for practical applications of CRVW.

6. Conclusions

In this paper, we have investigated the attenuation of evanescent Lamb waves guided in a CRVW defined by considering a sequence of coupled defect cavities in a phononic plate with cross holes. The complex band structure, the FRF and the displacement fields were calculated by considering the K–V model. An experiment was also conducted to verify the numerical results, using a scanning laser vibrometer. Besides, we devised two theoretical models to predict the spatial decay of evanescent Bloch waves inside the bandgap and inside a guidance frequency range for out-of-plane waves. Numerical and experimental results show that due to viscosity, guided Lamb waves are spatially evanescent. Guided evanescent Lamb waves are strongly confined and show rapid attenuation along the waveguide axis. The propagation and the attenuation of guided waves are correctly characterized by the K–V model. The displacement distribution can further be accurately predicted by considering only either the first or the first two least evanescent Bloch waves that are identified in the complex band structure. The results presented are expected to be useful for practical applications of highly confined viscoelastic phononic waveguides, for instance the directional mitigation of unwanted waves emitted by a source of elastic waves. In addition to the viscoelastic waveguides considered in this paper, it would be valuable to extend the analysis to viscoelastic couplers. We plan to conduct such research in future studies.

CRediT authorship contribution statement

Yu-Ke Ma: Software, Experiment, Writing – Original Draft. **Wei Guo:** Methodology, Software. **Yi-Ming Cui:** Experiment. **Yan-Feng Wang:** Conceptualization, Supervision, Writing – Reviewing and Editing. **Vincent Laude:** Writing – Reviewing and Editing. **Yue-Sheng Wang:** Writing – Reviewing and Editing.

Declaration of competing interest

The authors declare that they have no known competing financial interests or personal relationships that could have appeared to influence the work reported in this paper.

Acknowledgments

Financial support from the National Natural Science Foundation of China (12122207, 12021002 and 11991032) is gratefully acknowledged. V.L. acknowledges support from the EIPHI Graduate School (ANR-17-EURE-0002).

Appendix. Frequency response function obtained under the elastic model

In additional to the K–V model, the elastic model was also considered to calculate the FRF. Numerical results obtained by both models on the third to the sixth defects are plotted in Fig. 7(a) to (d). The black dot line is added to assist in comparing FRFs estimated on different

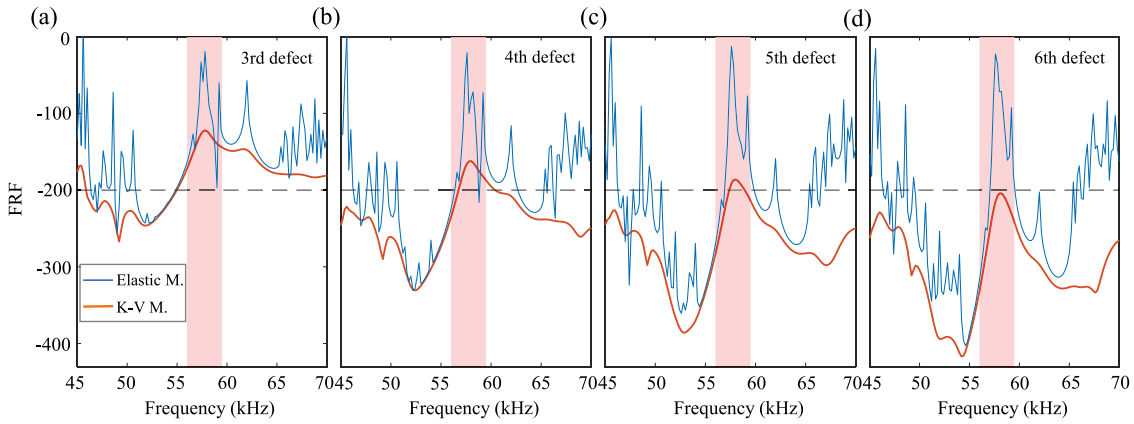

Fig. 7. FRFs obtained from distinct receiving regions of CRVW in simulation. Panel (a)–(d) present the numerical results on the third to six defects calculated including the K–V model and elastic model with the yellow and blue lines, respectively.

receiving regions. Many peaks in the elastic FRF are washed out in the viscoelastic FRF, because of attenuation. As the receiving region moves farther away, the elastic FRF inside the bandgap decreases, isolating more and more the guidance frequency range. The latter response changes little with distance, indicating guidance without attenuation. Conversely, attenuation is clearly seen inside the guidance frequency range for the viscoelastic FRF.

Data availability

Data will be made available on request.

References

[1] Kushwaha MS, Halevi P, Dobrzynski L, Djafari-Rouhani B. Acoustic band structure of periodic elastic composites. Phys Rev Lett 1993;71:2022.
[2] Wang Y-F, Wang Y-Z, Wu B, Chen W, Wang Y-S. Tunable and active phononic crystals and metamaterials. Appl Mech Rev 2020a;72:040801.
[3] Yang Z, Dai H, Chan N, Ma G, Sheng P. Acoustic metamaterial panels for sound attenuation in the 50–1000 hz regime. Appl Phys Lett 2010;96.
[4] Dong E, Cao P, Zhang J, Zhang S, Fang NX, Zhang Y. Underwater acoustic metamaterials. Natl. Sci. Rev. 2023;10:nwac246.
[5] Khelif A, Aoubiza B, Mohammadi S, Adibi A, Laude V. Complete band gaps in two-dimensional phononic crystal slabs. Phys Rev E 2006;74:046610.
[6] Laude V, Wilm M, Benchabane S, Khelif A. Full band gap for surface acoustic waves in a piezoelectric phononic crystal. Phys Rev E 2005;71:036607.
[7] Veres IA, Berer T, Matsuda O. Complex band structures of two dimensional phononic crystals: Analysis by the finite element method. J Appl Phys 2013;114:083519.
[8] Sigalas M, Economou EN. Band structure of elastic waves in two dimensional systems. Solid State Commun 1993;86:141.
[9] Qiu C, Liu Z. Acoustic directional radiation and enhancement caused by band-edge states of two-dimensional phononic crystals. Appl Phys Lett 2006;89.
[10] Liu Z, Zhang X, Mao Y, Zhu Y, Yang Z, Chan CT, Sheng P. Locally resonant sonic materials. Science 2000;289:1734.
[11] Jin Y, Jia X-Y, Wu Q-Q, He X, Yu G-C, Wu L-Z, Luo B. Design of vibration isolators by using the bragg scattering and local resonance band gaps in a layered honeycomb meta-structure. J Sound Vib 2022;116721.
[12] Laude V, Achaoui Y, Benchabane S, Khelif A. Evanescent bloch waves and the complex band structure of phononic crystals. Phys Rev B 2009;80:092301.
[13] Wang Y-F, Wang Y-S, Laude V. Wave propagation in two-dimensional viscoelastic metamaterials. Phys Rev B 2015;92:104110.
[14] Martínez-Sala R, Sancho J, Sánchez JV, Gómez V, Llinares J, Meseguer F. Sound attenuation by sculpture. Nature 1995;378:241.
[15] García-Chocano VM, Cabrera S, Sánchez-Dehesa J. Broadband sound absorption by lattices of microperforated cylindrical shells. Appl Phys Lett 2012;101:184101.
[16] Xiao X, He Z, Li E, Cheng A. Design multi-stopband laminate acoustic metamaterials for structural-acoustic coupled system. Mech Syst Signal Process 2019;115:418.
[17] Badreddine Assouar M, Senesi M, Oudich M, Ruzzene M, Hou Z. Broadband plate-type acoustic metamaterial for low-frequency sound attenuation. Appl Phys Lett 2012.
[18] Kushwaha MS. Stop-bands for periodic metallic rods: Sculptures that can filter the noise. Appl Phys Lett 1997;70:3218.
[19] Lee KY, Jeon W. Hierarchical phononic crystals for filtering multiple target frequencies of ultrasound. Sci Rep 2020;8070.
[20] Khelif A, Choujaa A, Djafari-Rouhani B, Wilm M, Ballandras S, Laude V. Trapping and guiding of acoustic waves by defect modes in a full-band-gap ultrasonic crystal. Phys Rev B 2003;68:214301.
[21] Jo S-H, Yoon H, Shin YC, Choi W, Park C-S, Kim M, Youn BD. Designing a phononic crystal with a defect for energy localization and harvesting: Supercell size and defect location. Int J Mech Sci 2020;179:105670.
[22] Wu L-Y, Chen L-W, Liu C-M. Acoustic energy harvesting using resonant cavity of a sonic crystal. Appl Phys Lett 2009.
[23] Zhang X, Li Y, Wang Y, Jia Z, Luo Y. Narrow-band filter design of phononic crystals with periodic point defects via topology optimization. Int J Mech Sci 2021a;212:106829.
[24] Jo S-H, Yoon H, Shin YC, Youn BD. Revealing defect-mode-enabled energy localization mechanisms of a one-dimensional phononic crystal. Int J Mech Sci 2022;215:106950.
[25] Wu F, Hou Z, Liu Z, Liu Y. Point defect states in two-dimensional phononic crystals. Phys Lett A 2001;292:198.
[26] Wang Y-F, Yang L, Wang T-T, Chen A-L, Laude V, Wang Y-S. Guided lamb waves in reconfigurable phononic crystal waveguides. Apl Mater 2021;9:081110.
[27] Fang K, Matheny MH, Luan X, Painter O. Optical transduction and routing of microwave phonons in cavity-optomechanical circuits. Nature Photonics 2016;10:489.
[28] Wang Y-F, Wang T-T, Liang J-W, Wang Y-S, Laude V. Channeled spectrum in the transmission of phononic crystal waveguides. J Sound Vib 2018a;437:410.
[29] Wang Y-F, Laude V, Wang Y-S. Coupling of evanescent and propagating guided modes in locally resonant phononic crystals. J Phys D: Appl Phys 2014;47:475502.
[30] Laude V. Principles and properties of phononic crystal waveguides. Apl Mater. 2021;9.
[31] Nomura M, Laude V, Maldovan M. Phononic crystals at various frequencies. Apl Mater. 2022;10.
[32] Guo W, Ma Y-K, Wang Y-F, Laude V, Wang Y-S. Dual-tunable phononic waveguides for manipulation of guided lamb waves. Programmable Mater. 2023;e11.
[33] Wang Y-F, Wang T-T, Liu J-P, Wang Y-S, Laude V. Guiding and splitting lamb waves in coupled-resonator elastic waveguides. Compos Struct 2018b;206:588.
[34] Wang T-T, Bargiel S, Lardet-Vieudrin F, Wang Y-F, Wang Y-S, Laude V. Collective resonances of a chain of coupled phononic microresonators. Phys Rev Appl 13:014022.
[35] Shi Y, Sha Z, Xu S, Zhang Y, Su G, Li B, Liu Y. Compact functional elastic waveguides based on confined mode. Extreme Mech Lett 2022;101919.
[36] Hatanaka D, Dodel A, Mahboob I, Onomitsu K, Yamaguchi H. Phonon propagation dynamics in band-engineered one-dimensional phononic crystal waveguides. New J Phys 2015;113032.
[37] Georgiades E, Lowe MJ, Craster RV. Computing leaky lamb waves for waveguides between elastic half-spaces using spectral collocation. J Acoust Soc Am 2024;629.
[38] H-wJi, Yang F, A-qQi, Wu X, Lv B, Ni J. Tunable coupled-resonator acoustic waveguides based on defect resonance body. Appl Phys A 2022;573.
[39] Cha J, Daraio C. Electrical tuning of elastic wave propagation in nanomechanical lattices at mhz frequencies. Nature Nanotechnol 2018;1016.
[40] Jiang Z, Zhou Y, Zheng S, Liu J, Xia B. Waveguides induced by replacing defects in phononic crystal. Int J Mech Sci 2023.
[41] Hatanaka D, Mahboob I, Onomitsu K, Yamaguchi H. Phonon waveguides for electromechanical circuits. Nature Nanotechnol 2014;520.
[42] Wang T-T, Wang Y-F, Deng Z-C, Laude V, Wang Y-S. Reconfigurable coupled-resonator acoustoelastic waveguides in fluid-filled phononic metaplates. Compos Struct 2023;116355.

[43] Hussein MI, Frazier MJ. Band structure of phononic crystals with general damping. J Appl Phys 2010;108.
[44] Moiseyenko RP, Laude V. Material loss influence on the complex band structure and group velocity in phononic crystals. Phys Rev B 2011;83:064301.
[45] Frazier MJ, Hussein MI. Generalized bloch's theorem for viscous metamaterials: Dispersion and effective properties based on frequencies and wavenumbers that are simultaneously complex. Comptes R Physique 2016;17:565.
[46] Zhang S-Y, Wang Y-F, Wang Y-S. Evanescent surface acoustic waves in 1d viscoelastic phononic crystals. J Appl Phys 2021b;129.
[47] Liu X-N, Hu G-K, Huang G-L, Sun C-T. An elastic metamaterial with simultaneously negative mass density and bulk modulus. Appl Phys Lett. 2011;98.
[48] Zhang S-Y, Luo J-C, Wang Y-F, Laude V, Wang Y-S. Evanescent waves in hybrid poroelastic metamaterials with interface effects. Int J Mech Sci 2023;247:108154.
[49] Brunet T, Merlin A, Mascaro B, Zimny K, Leng J, Poncelet O, Aristégui C, Mondain-Monval O. Soft 3d acoustic metamaterial with negative index. Nature Mater 2015;14:384.
[50] Dal Poggetto VF, Miranda Jr. EJ, Dos Santos JMC, Pugno NM. Wave attenuation in viscoelastic hierarchical plates. Int J Mech Sci 2022;107763.
[51] Laude V, Escalante JM, Martínez A. Effect of loss on the dispersion relation of photonic and phononic crystals. Phys Rev B 2013;88:224302.
[52] Manimala JM, Sun C. Microstructural design studies for locally dissipative acoustic metamaterials. J Appl Phys 2014;115:023518.
[53] Hu G, Tang L, Das R, Gao S, Liu H. Acoustic metamaterials with coupled local resonators for broadband vibration suppression. AIP Adv 2017;7.
[54] Hwan Oh J, Jae Kim Y, Young Kim Y. Wave attenuation and dissipation mechanisms in viscoelastic phononic crystals. J Appl Phys 2013;113.
[55] Yip KL, John S. Sound trapping and waveguiding in locally resonant viscoelastic phononic crystals. Sci Rep 2023;13:15313.
[56] Barnhart MV, Xu X, Chen Y, Zhang S, Song J, Huang G. Experimental demonstration of a dissipative multi-resonator metamaterial for broadband elastic wave attenuation. J Sound Vib 2019;438:1.
[57] Nouh M, Aldraihem O, Baz A. Vibration characteristics of metamaterial beams with periodic local resonances. J Vib Acoust 2014;136.
[58] Nouh M, Aldraihem O, Baz A. Wave propagation in metamaterial plates with periodic local resonances. J Sound Vib 2015;341:53.
[59] Miniaci M, Krushynska A, Gliozzi AS, Kherraz N, Bosia F, Pugno NM. Design and fabrication of bioinspired hierarchical dissipative elastic metamaterials. Phys Rev Appl 2018;10:024012.
[60] Bulıcek M, Málek J, Rajagopal K. On Kelvin–Voigt model and its generalizations. Evol Equ Control Theory 2012;1:17.
[61] Krushynska A, Kouznetsova V, Geers M. Visco-elastic effects on wave dispersion in three-phase acoustic metamaterials. J Mech Phys Solids 2016;96:29.
[62] Krushynska AO, Gliozzi AS, Fina A, Krushinsky D, Battegazzore D, Badillo-Ávila MA, Acuautla M, Stassi S, Noè C, Pugno NM, et al. Dissipative dynamics of polymer phononic materials. Adv Funct Mater 2021;31:2103424.
[63] Othmani C, Dahmen S, Njeh A, Ghozlen MHB. Investigation of guided waves propagation in orthotropic viscoelastic carbon–epoxy plate by legendre polynomial method. Mech Res Commun 2016;27.
[64] Takali F, Othmani C. Viscoelastic rheological models for guided acoustic waves: Single mode at high frequency and second harmonic generation of lamb and sh modes. Math Methods Appl Sci 2022;11875.
[65] Guo W, Zhang S-Y, Wang Y-F, Laude V, Wang Y-S. Evanescent lamb waves in viscoelastic phononic metastrip. Int J Mech Sci 2022;236:107748.
[66] Wang Y-F, Wang T-T, Liang J-W, Wang Y-S, Laude V. Channeled spectrum in the transmission of phononic crystal waveguides. J Sound Vib 2018c;437:410.